Multi-compartment model for heat and mass transfer during the frying of frozen pre-fried french fries

Têko Gouyo, Daniel Goujot, Philippe Bohuon, Francis F. Courtois

Multi-compartment model for heat and mass transfer during the frying of frozen pre-fried french fries

Têko Gouyo[a,b], Daniel Goujot[c], Philippe Bohuon[a,*], Francis Courtois[a]

[a] *QualiSud, Univ Montpellier, Avignon Université, CIRAD, Institut Agro, IRD, Université de La Réunion, Montpellier, France*

[b] *SEB, Ecully-Food Science; 112 Chemin du Moulin Carron, 69130 Écully, France*

[c] *Université Paris-Saclay, INRAE, AgroParisTech, UMR SayFood, 91300, Massy, France*

Abstract

This paper develops a model for hot-air frying of frozen pre-fried french fries. A dynamic three-compartment model including heat and vapour transfer was developed. The model takes into account four major stages: defrosting, warm-up, convective drying and boiling drying. X-ray microtomographic observations led to the assumption of a compartmental structure: a central compartment (#1) with a high water content, a peripheral compartment (#3) corresponding to the dry crust and an intermediate compartment (#2) filled with vapour which appears during frying. The model was validated against experimental measurements: french fries core temperature, and average water content. Validations were made on three different hot-air frying conditions (combining convection and radiation). Heat transfer coefficient (ranging from 66 — 76 $W{\cdot}m^{-2}{\cdot}K^{-1}$) and water transfer coefficient (ranging from 0.0035 — 0.0040 $m{\cdot}s^{-1}$) were identified. This model represented well enough the behaviour of french fries from defrosting to boiling drying to be used as a performant numerical tool to control and optimize hot-air frying.

Keywords: Frying ; Drying ; Modelling ; Heat transfer ; French fries ; Mass transfer

1. Introduction

French fries are solid with a core, which is moist and soft, and a crispy outer dry crust of approximately 0.5 — 1.5 mm (Bouchon and Aguilera, 2001; Pedreschi and Aguilera, 2002). French fries are popular potato products in many countries because of their structure and attractive texture (Garayo and Moreira, 2002). Deep-fat frying can be defined as a process of drying and cooking through contact with hot oil. This process essentially consists of soaking the product in hot vegetable oil at a temperature above the boiling point of water, typically 150—180 °C. These frying conditions lead to high rates of heat and mass transfer, causing water loss and oil uptake, with consequent changes in taste, texture and colour properties.

The main disadvantage of consuming deep-fat fries, and in general all deep-fat fried products, is related to their high fat content (about 20 — 40 g oil/100 g fat-free dry matter) (Garayo and Moreira, 2002). While the oil gives their specific flavour to fried products, consumers tend to move towards lower-fat food products, leading to reduce fat in product during food processing. A great deal of research have been done for years to develop fried food products with reduced fat content. Consequently, many studies on the mechanisms of fat absorption during frying have been carried out considering different pre-treatment and deep-fat frying conditions (Bouchon and Pyle, 2005; Debnath

*Philippe Bohuon

Email addresses: teko.gouyo@cirad.fr (Têko Gouyo), daniel.goujot@agroparistech.fr (Daniel Goujot), philippe.bohuon@supagro.fr (Philippe Bohuon)

et al., 2009; Dueik et al., 2010; Vauvre et al., 2014; van Koerten et al., 2015).

Over in the past decade, hot-air fryers have been developed to prevent the high oil uptake during the production of deep-fat fries. The objective is to reduce oil uptake when consuming french fries. The hot-air frying aims to produce a "fried product" by sparging, essentially, hot-air around the material instead of immersing it in hot oil (Andrés et al., 2013; Heredia et al., 2014; Sansano et al., 2015; Teruel et al., 2015; Tian et al., 2017). The hot-air frying creates the frying effect by bringing direct contact between a fine mist of oil droplets in hot-air and the product, inside the hot-air fryer. These hot-air fryers are designed to provide high heat transfer from the air to the fried product either by simple forced convection or by a combination of forced convection and radiation or conduction. The amount of oil used is significantly less than that used in deep-fat frying, resulting in very low fat products (1.12 g oil/100 g defatted dry matter) (Teruel et al., 2015).

The current disadvantage of this type of fryer is that it is the site of less intense heat and mass transfer than deep-fat frying, thus generating fries with textures far from those obtained by deep-fat frying (Teruel et al., 2015). Heat transfer rates involved in deep-fat frying are in particular higher than those encountered with other heat vectors such as gas (e.g., hot-air, superheated steam). Besides, when the product is surrounded with oil (immersed product), heat is transferred almost uniformly to the product (Sumnu and Sahin, 2008). This feature is more difficult to achieve with alternative cooking or frying processes such as hot-air frying or infrared heating. During deep-fat frying at 180 °C, the values of heat transfer coefficient between the hot-oil and the product surface can be as high as 5000 $W{\cdot}m^{-2}{\cdot}K^{-1}$ according to van Koerten et al. (2015), 650 $W{\cdot}m^{-2}{\cdot}K^{-1}$ according to Costa et al. (1999) and 1100 $W{\cdot}m^{-2}{\cdot}K^{-1}$ according to Hubbard and Farkas (1999). Whereas in hot-air frying, the values do not exceed 100 $W{\cdot}m^{-2}{\cdot}K^{-1}$ (Andrés et al., 2013) due to the low thermal conductivity of air.

During frying, the formation of a crust is the result of transformations in the native structure of the potato caused by heat and mass transfer (Pedreschi and Aguilera, 2002; Pedreschi, 2009). The structure of the core and crust of a fried product is affected by the time-temperature combination and the frying process. Therefore, a better understanding of the transport processes (heat and mass) and their relationship to various operating parameters should make it possible to optimize the frying process and thus improve hot-air fries. The process optimization can be achieved using the mathematical model which is based on fundamental physical principles.

The development of mathematical models to describe deep-fat frying process has been the subject of several research studies in the past. Various models have been developed to describe heat and mass transfer during deep-fat frying, with a complexity ranging from simplified empirical equations to complex numerical models, which incorporate mechanistic equations for both heat and mass transfer. All models have their own advantages in describing the water loss during frying. Among the models used, the following can be mentioned: single zone model (Dincer and Yildiz, 1996; Grenier et al., 2010), double zone model (two distinguished regions: core and crust) (Farkas et al., 1996; Farid and Chen, 1998; Bouchon and Pyle, 2005), multiphase porous media model (Xiong et al., 1992; Ni and Datta, 1999; Yamsaengsung and Moreira, 2002) and compartmental dynamic model (Courtois et al., 1998; Costa and Oliveira, 1999). On hot-air frying, no studies have been carried out on the modeling of frozen french fries. To date, there is only one scientific publication (Andrés et al., 2013) which measured the kinetics of mass transfer and volume changes in hot-air frying and deep-fat frying at the temperature (180 °C) and concluded that both were affected by medium type.

The aim of this work is to build-up a dynamic model for the hot-air frying of frozen pre-fried french fries, to be able to simulate both heat and mass transfer for control and optimization purposes. To represent the internal gradients (water and temperature), the french fries were modelled as three concentric compartments in series, with heat and mass resistances at interfaces only.

2. Materials and methods

2.1. Raw materials and frying equipment

The experiments were carried out with commercial frozen pre-fried (Vauvre et al., 2014; Aguilera and Gloria-Hernandez, 2000) french fries (Mc-Cain Tradition) purchased at a local supermarket and stored in a cold room at -18 °C. These French fries (Mccain tradition) are designed for domestic deep fat frying of 5 to 10 minutes. A primary selection of frozen french fries was done, according to (1) being straight, (2) with a square section of 9 × 9 mm exactly, and (3) more long than 60mm. Selected frozen french fries were resized to 60 mm in length with a specific cutter. Hot-air fryer equipment (Airfryer Philips XL HD9240/90, Avance Collection, Amsterdam, The Netherlands) with a power of 2100 W was used. A specific fryer's control system allowed to regulate the air velocity and to add an extra radiative heating component (halogen, Suney 012072, 1000 W). The air velocity was measured above the basket with an anemometer (MiniAir 64 Mini, OmniInstruments, UK). This modification allowed for three different operating conditions in terms of the intensity of energy input and the mode of input. The fryer was instrumented with a power meter (PM231 – Powermeter, brennenstuhl, CHINA) connected to the energy sources (electrical resistance and radiative heating source).

For each experiment, a single bed of 0.200 kg of french fries was placed in the cooking basket. The different sides of the fries hardly touch each other. Triplicates were performed for each experiment. Once in the middle of the frying process, the French fries were stirred to homogenize the heat treatment of all sides of the French fries.

2.2. Water content

In order to determine the amount of water evaporated from the potato during frying, the fryer was placed on a scale (Sartorius CPA34001S, France, with a capacity of 34 kg and a precision of 10^{-4} kg) that allowed recording at 1 Hz of the water loss. The end of the frying process was when the water loss reached 45 %. After frying, the water content of the french fry was determined by oven drying at 105 °C to constant weight (approximately 24 h).

2.3. Temperature measurements

Different temperatures were measured during the frying process. Thermocouples (type J, Temp-control, Manchester, UK) were used for the temperature measurements. Associated uncertainty was estimated to be ± 0.5 °C. A thermocouple was inserted in the potato, either at the surface (T_s) or at the core (T_{co}). Infrared thermometers (MLX90614KSF-ACC, Melexis, Corbeil-Essonnes, France), were also used to measure the surface temperature of french fries directly in contact with hot-air (T_{IR}). The air temperature (T_a) away from the french fries was also measured with a thermocouple type J placed in the Airfryer.

3. Model development

3.1. Compartments: experimental justification

The experimental observation of frozen french fries during hot-air frying by X-ray microtomography by Gouyo et al. (2021)(figure 1a) shows a central compartment with a pre-crust formed at the periphery of the frozen french fry. At the end of frying, three distinct compartments were observed: the core has shrunk while an intermediate gaseous one has appeared.

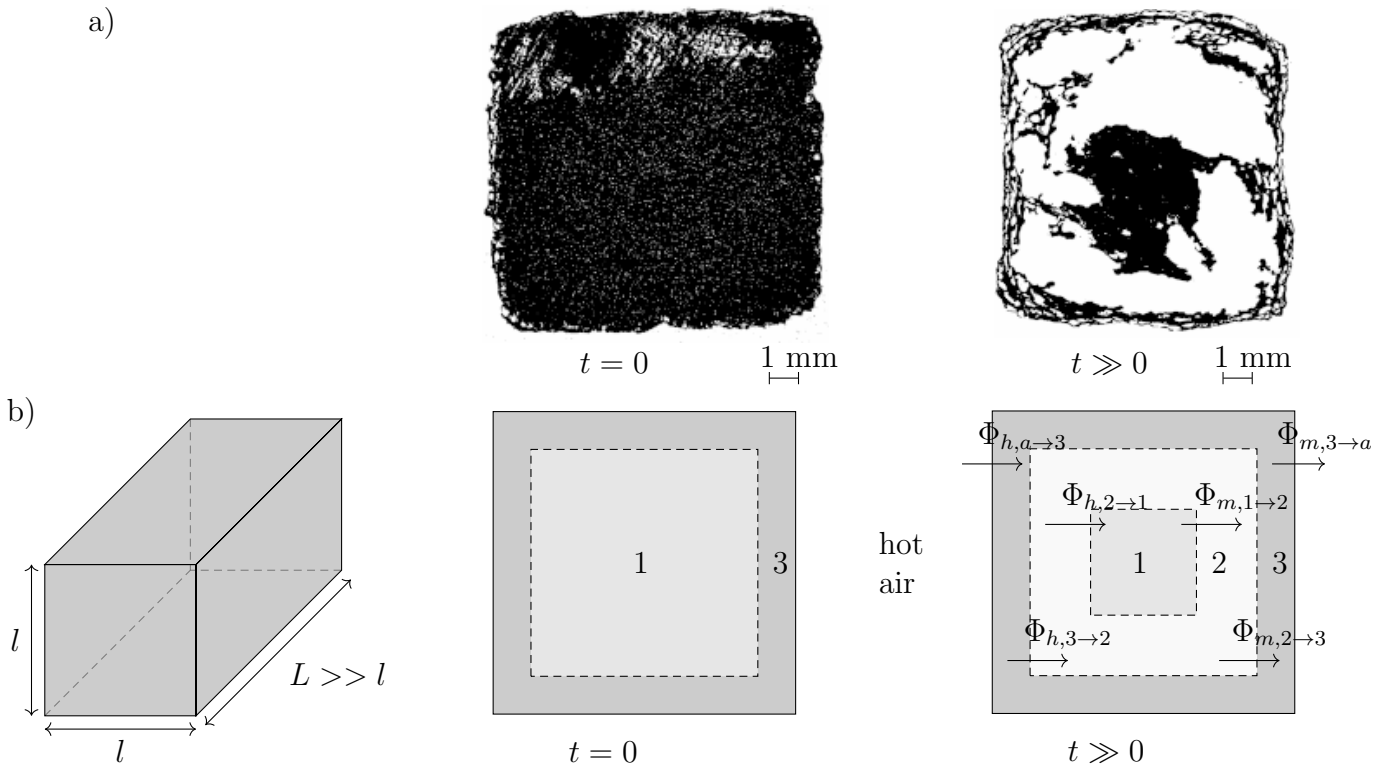

Figure 1: a)French fry cross-sectional slices obtained from X-ray microtomography analysis (Gouyo et al., 2021); b)French fries are seen as infinite rectangular of square section with 3 compartments (the second compartment being negligible at $t = 0$). Heat flux density (ϕ_h) and vapor flux density (ϕ_m) are transferred between these compartments.

Based on these findings, the chosen model consider the french fries as composed by 3 different compartments (figure 1):

1. the central compartment #1, containing dry (fatted) matter (intrinsic density ρ_{dfm1}) and water, with decreasing volume and high water content. Its water content X_1 (in kg water per kg dry fatted matter) is the sum, with $X_1 = W_1 + I_1$, of the state variables ice content I_1 and liquid water content W_1. Other state variables are temperature T_1 (Celsius degrees), and the shrinking volume V_1.

2. the medium compartment #2, of volume V_2, which appears during frying around the core of the fry, is filled of m_2 (in kg) of vapor possibly superheated at temperature T_2 that escaped from compartment #1. There is no solid or liquid in compartment #2.

3. the peripheral compartment #3 corresponds to the pre-existing crust region in the frozen french fries. This pre-crust has already formed as a result of the normal pre-frying process producing

the frozen french fries. It is a porous dry (fatted) matter (intrinsic density ρ_{dfm3}, constant volume V_3) with water, with very low water content and higher oil content. Its water content X_3 (in kg water per kg dry fatted matter) is the sum, with $X_3 = W_3 + I_3$, of the state variables ice content I_3 and liquid water content W_3. Temperature T_3 is another state variable.

Hence state variables are W_1, W_3, I_1, I_3, T_i ($i = 1, 2$ or 3) and V_2 and m_2. External variables are air temperature (T_a) and air water content (Y_a).

3.2. General assumptions

To minimise computational effort, several assumptions were made for development of the model.

- Water transfer in vapour state.
- According to our experimental data (Gouyo et al., 2021), the shrinkage of frozen french fries during frying was very low ($< 7\%$), hence the total volume $V = V_1 + V_2 + V_3$ is assumed constant. The volume V_3 of compartment #3 and its thickness l_3 were assumed constant, because experimental measurements of on one hand the pre-crust and on the other hand the final French fries crust, carried out with a calliper and a microtomography measurement, showed that their thickness varies, on the one hand, between 0.7 and 1.4 mm, and on the other hand, between 0.5 and 1.5 mm. Hence its dry fatted matter density ρ_{dfm3} has also been considered constant as well, and the sum $V_1 + V_2$ was also considered constant.
- The convective/diffusive drying and the boiling drying first occur in compartment #3.
- Shrinkage of dry fatted matter of compartment #3 was assumed to be negligible according to experimental data.
- The vapour transfer through compartment #3 was assumed to follow Darcy's law (Loncin and Merson, 1979) and the vapour accumulation in compartment #3 was assumed to be negligible.
- Intermediate compartment #2 makes no resistance to vapour transfer, only to heat transfer.
- In compartments #1, the convection-diffusion drying prior to boiling is considered to be negligible.
- Defrosting was assumed to occur at 0°C just like pure water.
- The vapour is only transferred outwards from the product.
- Total pressure P_a in compartments #1 and #3 is constant and equal to atmospheric pressure.

The evolution of the different variables are summarized in Table 1. The different successive mechanisms taken into account in the model are listed as well.

Table 1: Sum-up of successive mecanisms and results on the evolution of the variables.

Conditions	Step	Variables values and evolutions													
		Compartment #1					Compartment #2				Compartment #3				
T (°C)		T_1	V_1	P_1	I_1	W_1	T_2	V_2	P_2	m_2	T_3	V_3	P_3	I_3	W_3
$T_1 < 0$ $T_3 < 0$	warm-up #1 and #3	↗	∼	$= P_a$	∼	∼	n/a	$= 0$	n/a	n/a	↗	∼	$= P_a$	∼	∼
$T_1 < 0$ $T_3 = 0$	warm-up #1 defrost #3	↗	∼	$= P_a$	∼	∼	n/a	$= 0$	n/a	n/a	$= 0$	∼	$= P_a$	↘	↗
$T_1 < 0$ $0 < T_3 < 100$	warm-up #1 drying #3	↗	∼	$= P_a$	∼	∼	n/a	$= 0$	n/a	n/a	↗	∼	$= P_a$	$= 0$	↘
$T_1 = 0$ $0 < T_3 < 100$	defrost #1 drying #3	$= 0$	∼	$= P_a$	↘	↗	n/a	$= 0$	n/a	n/a	↗	∼	$= P_a$	$= 0$	↘
$0 < T_1 < 100$ $0 < T_3 < 100$	warm-up #1 drying #3	↗	∼	$= P_a$	↘	∼	n/a	$= 0$	n/a	n/a	↗	∼	$= P_a$	$= 0$	↘
$0 < T_1 < 100$ $T_3 \geq 100$	drying #1 *boiling#3*	↗	∼	$= P_a$	$= 0$	∼	n/a	$= 0$	n/a	n/a	↗	∼	$= P_a$	$= 0$	↘
$T_1 \geq 100$ $T_3 \geq 100$	*boiling* #1 and #3	↗	↘	$= P_a$	$= 0$	↘	↗	↗	↗	↗	↗	∼	$= P_a$	$= 0$	↘

∼: constant value, ↗: grow, ↘: decrease and n/a: not available (until compartment #2 exists)

3.3. Geometry and compartment properties

A few geometry assumptions are necessary to relate volume shrinkage, external surface area, and pressure gradient in compartment #3. Minimal assumptions were: shape is globally an infinite rectangle of square section (figure 1). A finite rectangle of square section $l \cdot l$ and length L was assumed. Hence the volume is $V = l^2 \cdot L$ and the external surface area is $A_{3,a} = 4 \cdot l \cdot L + 2 \cdot l^2$. Compartment #3 is assumed to keep a constant thickness l_3. In compartmental models, each compartment is assumed to be uniform in water content (X, I, W), temperature (T), pressure (P), heat capacity of dry fatted matter (Cp_{dfm}), dry fatted matter density (ρ_{dfm}), ... whenever applicable (no ρ_{dfm} in compartment #2).

In addition, heat capacities of dry fatted matter (Cp_{dfm}) and dry fatted matter densities (ρ_{dfm}) are constant over time as long as volume remains constant. In practice, only ρ_{dfm1} varied when volume V_1 of compartment #1 shrinked (because of boiling).

3.4. Shrinkage of compartment #1

By microstructure analysis of french fries, Gouyo et al. (2021) showed that the porosity created in the frozen french fry matched the water loss of the product. The same analogy was made for the water loss in compartment #1. The volume of water loss corresponds to the volume of V_2 created so as to get the initial volume of compartment #1 : $V_{1/0}$=V_1 +V_2. It was considered that ice and water have similar volumes in the product and that shrinkage was ideal, hence we can write:

$$\frac{V_1}{V_{1/0}} = a \cdot \frac{X_1}{X_{1/0}} \tag{1}$$

where $V_{1/0}$ and $X_{1/0}$ are respectively the volume and the water content of compartment #1 at time 0 and $a = 1$ is the dimensionless parameter for the linear relationship. Deriving previous expression

leads to:

$$\frac{dV_1}{dt} = V_{1/0} \cdot a \cdot \frac{\frac{dX_1}{dt}}{X_{1/0}} \tag{2}$$

which can be shorten as:

$$\frac{dV_1}{dt} = k_v \cdot \frac{dX_1}{dt} \tag{3}$$

Note that, for compartment #2, we can write (since $V_1 + V_2$ is constant):

$$\frac{dV_2}{dt} = -\frac{dV_1}{dt} = -k_v \cdot \frac{dX_1}{dt} \tag{4}$$

3.5. Density of dry fatted matter (ρ_{dfm})

ρ_{dfm} is expressed in kg of dry fatted matter per m^3 of total compartment volume *e.g.* m/V. Shrinkage of this dry fatted matter was ignored, leading to constant value for ρ_{dfm3} with respect to time. This is true for ρ_{dfm1} only before compartment #1 boils (boiling leads to shrinking volume V_1, and increasing ρ_{dfm1}). It should be emphasized that these two parameters may not be equal since crust may have a different oil content. If we denote $\rho*$, the true bulk density (related to true volume of matter), we have the following equalities:

$$\frac{1}{\rho_{dfm1}} = \frac{X_1}{\rho_w*} + \frac{1}{\rho_{dfm1}*} \tag{5}$$

$$\frac{1}{\rho_{dfm3}} = \frac{X_3}{\rho_w*} + \frac{1}{\rho_{dfm3}*} \tag{6}$$

where ρ_w* is the intrinsic density of pure water, $\rho_{dfm1}*$ and $\rho_{dfm3}*$ are the core and crust bulk densities.

3.6. Average water content (X_m) and water activity (Aw)

We assume the water vapour contained in the compartment #2, at the time of measurement, is negligible. The only water accounted for is located in the two other compartments, hence:

$$X_m = \frac{\rho_{dfm1/0} \cdot V_{1/0} \cdot X_1 + \rho_{dfm3} \cdot V_3 \cdot X_3}{\rho_{dfm1/0} \cdot V_{1/0} + \rho_{dfm3} \cdot V_3} \tag{7}$$

Note that, compartment #2 is either null (non existent) or composed exclusively of pure water vapour, hence, its water activity is $P_{v2}/P_{vsat}(T_2)$.

As stated in Bassal et al. (1993) for potato starch, one could consider the following *Oswin* equation Oswin (1946), see Figure 2, which gives only about 6 % error of water content at equilibrium (noted X_{eq}):

$$X_{eq}(Aw, T) = \frac{1}{100} \cdot \left(\frac{Aw}{1 - Aw}\right)^{r_q + r_t \cdot T} \cdot (r_l + r_n \cdot T) \tag{8}$$

where $r_l = 14.11$, $r_n = -5.013 \cdot 10^{-2}$, $r_q = 0.124$ and $r_t = 2.063 \cdot 10^{-3}$ (where T is in °C).

Note that, by definition, when the water boils in a compartment, we can write the boiling equilibrium as $Aw(X, T) \cdot P_{vsat}(T) = P_a$. The boiling curve T as function of X is obtained by writing $X = X_{eq}(P_a/P_{vsat}(T), T)$. One should note that compartment #2 is special since it is in gas phase (vapour) as opposed to the other two solid compartments.

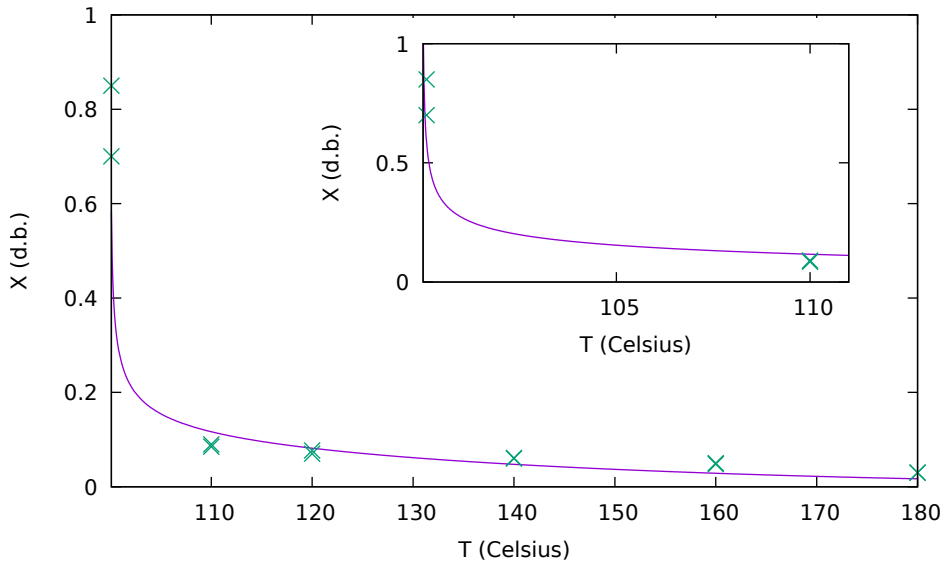

Figure 2: Boiling curve of potato starch. Green crosses: our experimental measurements; purple line: Oswin model $X_{eq}(Aw,T) = \frac{1}{100} \cdot \left(\frac{Aw}{1-Aw}\right)^{0.124+2.063\cdot10^{-3}\cdot T} \cdot (14.11 - 5.013 \cdot 10^{-2} \cdot T)$ based on (de)sorption model from Bassal et al. (1993) for potato starch at 115 °C (Murray, 1967).

3.7. Mass transfer

3.7.1. Convective drying (boundary equations)

Water flux density (in kg water per second and square meters) from compartment #3 to hot-air is under vapour phase and expressed as (positive in outward direction):

$$\phi_{m,3\to a} = k_{3,a} \cdot \frac{M_w}{R} \cdot \left(\frac{P_{v3}}{T_3 + T_\tau} - \frac{P_{va}\left(Y_a\right)}{T_a + T_\tau}\right) \tag{9}$$

where M_w is the molar mass of water, R is the ideal gas constant and $k_{3,a}$ the mass transfer coefficient ($m \cdot s^{-1}$). This relation is derived from the robust equation for ideal gas. The liquid/vapor equilibrium pressure at temperatures T_a in the oven (around 170°C when vapor is released from the french fries) is very high. This implies that HRa is negligible at these temperatures. Measurement confirmed HRa was 3% at most. At beginning of drying, T_a is much lower and HRa is not negligible, but the release of vapor from french fries is negligible at that point. Hence the effect of vapor relase from french fries has negligible consequences, and was not included in the model. It results in condensation at the beginning (non monotonous evolution with time). The subscript a stands for external air flowing to french fries (infinite reservoir) and Y is air water content, the partial pressure of vapour in air is $P_{va}(Y) = \dfrac{P_a \cdot Y}{M_{v/a} + Y}$ with P_a the total atmospheric pressure and the partial pressure of vapour in equilibrium with product is

$$P_v(X,T) = Aw(X,T) \cdot P_{vsat}(T). \tag{10}$$

Convective drying happens only in compartment #3 and only before its water boils. Compartment #2 cannot dry since it is composed of pure water vapour and compartment #1 is assumed to not dry until its water boils (*i.e.* when $T_1 \geq 100$°C). Hence, it was assumed that there was no direct water transfer ($k_{1,3} = 0$) between compartment #1 and compartment #3 until boiling occurs in compartment #1.

3.7.2. Boiling

When boiling occurs in compartment #1, both Clausius-Clapeyron relationship (Murray, 1967)

$$P_{vsat}(T) = P_{vsat0^oC} \cdot 10^{\frac{A \cdot T}{T+B}} \tag{11}$$

and Oswin equation (8) are valid, hence product water content, product temperature, and product water activity are all coupled together. We use the temperature of compartment 1 to parameterize the water activity and water content. From this temperature, the Clausius-Clapeyron relationship in above equation computes P_{vsat}; we then deduce the water activity of the product from the equilibrium equation

$$Aw(X_1, T_1) \cdot P_{vsat}(T_1) = P_a \tag{12}$$

then use Oswin's model (equation (8)) to compute the water content.

The mass transfer to the compartment #2 can be derived from the equilibrium equation (12):

$$\begin{aligned} \frac{dP_a}{dt} &= Aw(X_1, T_1) \cdot \frac{\partial P_{vsat}}{\partial T_1}(T_1) \cdot \frac{dT_1}{dt} \\ &\quad + P_{vsat}(T_1) \cdot \frac{\partial Aw}{\partial X_1}(X_1, T_1) \cdot \frac{dX_1}{dt} \\ &\quad + P_{vsat}(T_1) \cdot \frac{\partial Aw}{\partial T_1}(X_1, T_1) \cdot \frac{dT_1}{dt} \end{aligned} \tag{13}$$

Since P_a is assumed being a constant, equation (13) can be rewritten as:

$$\begin{aligned} \frac{dX_1}{dt} &= -\frac{Aw(X_1, T_1)}{P_{vsat}(T_1)} \cdot \frac{\partial P_{vsat}(T_1)}{\partial T_1} \cdot \left(\frac{\partial Aw(X_1, T_1)}{\partial X_1} \right)^{-1} \cdot \frac{dT_1}{dt} \\ &\quad - \frac{\partial Aw(X_1, T_1)}{\partial T_1} \cdot \left(\frac{\partial Aw(X_1, T_1)}{\partial X_1} \right)^{-1} \cdot \frac{dT_1}{dt} \\ &= -\left[\frac{Aw(X_1, T_1)}{P_{vsat}(T_1)} \cdot \frac{\partial P_{vsat}(T_1)}{\partial T_1} + \frac{\partial Aw(X_1, T_1)}{\partial T_1} \right] \cdot \left(\frac{\partial Aw(X_1, T_1)}{\partial X_1} \right)^{-1} \cdot \frac{dT_1}{dt} \\ &= f(X_1, T_1) \cdot \frac{dT_1}{dt} \end{aligned} \tag{14}$$

Hence flux density can be written as:

$$A_{1,2} \cdot \phi_{m,1 \to 2} = -\rho_{dfm1} \cdot V_1 \cdot \frac{dX_1}{dt} = -\rho_{dfm1} \cdot V_1 \cdot f(X_1, T_1) \cdot \frac{dT_1}{dt} \tag{15}$$

Computing the value of $f(X_1, T_1)$ is to be done with the derivatives of the inverse of Oswin equation

$$Aw(X, T) = \frac{1}{\left(\frac{r_l + r_n \cdot T}{100 \cdot X} \right)^{r_q + r_t \cdot T} + 1} \tag{16}$$

and with the following derivative of Clausius-Clapeyron relationship equation (11):

$$\frac{\partial P_{vsat}(T)}{\partial T} = \frac{\ln(10) \cdot A \cdot B}{(T+B)^2} \cdot P_{vsat}(T) \tag{17}$$

A similar approach gives, for compartment #3:

$$A_{3,a} \cdot \phi_{m,3\to a} = -\rho_{dfm3} \cdot V_3 \cdot \frac{dX_3}{dt} = -\rho_{dfm3} \cdot V_3 \cdot f(X_3, T_3) \cdot \frac{dT_3}{dt} \tag{18}$$

Compartment #2 also emits water vapor to air which is "filtrated" by compartment #3 following Darcy's law (Loncin and Merson, 1979). The equation is:

$$\phi_{m,2\to a} = \rho_v \cdot \frac{\kappa_v}{\mu} \cdot \overrightarrow{\nabla} P = \rho_v \cdot \frac{\kappa_v}{\mu \cdot l_3} \cdot (P_{v2} - P_{va}) \tag{19}$$

where κ_v is the intrinsic permeability of the compartment #3 medium to vapour (m^2), μ the dynamic viscosity of vapour (Pa·s), and l_3 the length over which the pressure drop is taking place (m). Assuming $P_{va} \approx P_a$ (pure vapor around the product), we get:

$$\phi_{m,2\to a} = \rho_v \cdot \frac{\kappa_v}{\mu \cdot l_3} \cdot (P_{v2} - P_a) \tag{20}$$

3.8. Heat transfer

All heat transfer between compartments and with air are assumed to be of convective type. Hence, heat flux densities can be written simply as:

$$\phi_{h,a\to 3} = h_{3,a} \cdot (T_a - T_3) \tag{21}$$

As long as compartment #1 is not boiling, there is no compartment #2 and direct heat transfer between compartment #1 and #3 is done by conduction:

$$\phi_{h,3\to 1} = h_{1,3} \cdot (T_3 - T_1) \tag{22}$$

When compartment #1 is boiling then, heat transfer is indirectly, by convection through compartment #2:

$$\phi_{h,2\to 1} = h_{1,2} \cdot (T_2 - T_1) \tag{23}$$

$$\phi_{h,3\to 2} = h_{2,3} \cdot (T_3 - T_2) \tag{24}$$

Note: It was assumed that $h_{1,2} = h_{2,3}$.

3.9. Frozen condition

It was assumed that there was no sublimation, the ice first becomes liquid water then vapour. To simplify equations, it was assumed that no (negligible) drying occurs in a compartment #i where ice content $I_i > 0$. X_i is the total water content (ice+liquid water) with respect to the dry fatted matter (dry matter + oil). I_i is the frozen water content, hence the liquid water content is equal to $W_i = X_i - I_i$.

4. Heat and mass balances

4.1. Internal compartment #1

4.1.1. Case 1: $I_1 > 0$, $T_1 < 0$

In this case, all the water is ice and remains at temperature below 0°C and no drying (sublimation) occurs, hence:

$$\frac{dI_1}{dt} = \frac{dW_1}{dt} = \frac{dX_1}{dt} = \frac{dV_1}{dt} = 0 \tag{25}$$

$$\rho_{dfm1} \cdot V_1 \cdot (Cp_{dfm1} + Cp_{ice} \cdot I_1 + Cp_w \cdot W_1) \cdot \frac{dT_1}{dt} = \phi_{h,3\to1} \cdot A_{1,3} \tag{26}$$

where $A_{1,3}$ is the section area between compartments #1 and #3 (equivalent to $A_{2,3}$ since compartment #2 does not exist).

4.1.2. Case 2: $I_1 > 0$, $T_1 = 0$

In this case, the temperature is stabilised at zero degrees until all the ice is transformed into liquid water:

$$\frac{dT_1}{dt} = 0 \tag{27}$$

All thermal energy taken from convection from compartment #3 is used to melt ice into liquid water:

$$\rho_{dfm1} \cdot V_1 \cdot \frac{d\left((Cp_{dfm1} + Cp_{ice} \cdot I_1 + Cp_w \cdot W_1) \cdot T_1\right)}{dt} = \phi_{h,3\to1} \cdot A_{1,3} + \rho_{dfm1} \cdot V_1 \cdot \frac{dI_1}{dt} \cdot L_{defrost} \tag{28}$$

Hence, we have

$$0 = \phi_{h,3\to1} \cdot A_{1,3} + \rho_{dfm1} \cdot V_1 \cdot \frac{dI_1}{dt} \cdot L_{defrost} \tag{29}$$

which gives the following relationship:

$$\rho_{dfm1} \cdot V_1 \cdot L_{defrost} \cdot \frac{dI_1}{dt} = -\phi_{h,3\to1} \cdot A_{1,3} \tag{30}$$

At the same time, the overall mass of compartment #1 is constant:

$$\frac{dX_1}{dt} = 0 \;\Rightarrow\; \frac{dW_1}{dt} = -\frac{dI_1}{dt} \tag{31}$$

as well as its volume:

$$\frac{dV_1}{dt} = k_v \cdot \frac{dX_1}{dt} = 0 \tag{32}$$

4.1.3. Case 3: $I_1 = 0$, $0 < T_1 < 100$

In this case, there is no more ice ($X_1 = W_1$) and the water mass transfer is assumed to be negligible (X_1 and V_1 are constant). The convective heat transfer is:

$$\rho_{dfm1} \cdot V_1 \cdot \frac{d\left((Cp_{dfm1} + Cp_w \cdot W_1) \cdot T_1\right)}{dt} = \phi_{h,3\to1} \cdot A_{1,3} \tag{33}$$

which can be simplified as:

$$\rho_{dfm1} \cdot V_1 \cdot (Cp_{dfm1} + Cp_w \cdot W_1) \cdot \frac{dT_1}{dt} = \phi_{h,3\to1} \cdot A_{1,3} \tag{34}$$

4.1.4. Case 4: $I_1 = 0$, $T_1 \geq 100$

In this case, the water ($X_1 = W_1$) can boil hence encounters no resistance to mass transfer. V_1 shrinks as X_1 decreases. In addition, since V_1 is no longer a constant, ρ_{dfm1} varies as well but the combination $V_1 \cdot \rho_{dfm1}$ remains constant since it is equal to the mass of dry fatted matter. The water mass transfer is driven only by the heat transfer as described by the following equation:

$$\rho_{dfm1} \cdot V_1 \cdot \frac{d\left((Cp_{dfm1} + Cp_w \cdot W_1) \cdot T_1\right)}{dt} = \phi_{h,2\to1} \cdot A_{1,2} - \phi_{m,1\to2} \cdot A_{1,2} \cdot (L_v + Cp_v \cdot T_1) \tag{35}$$

In addition, two algebraic conditions must be respected. First is the shrinkage of V_1 as stated in equation 1 and, second is the boiling curve to follow:

$$Aw(W_1, T_1) \cdot P_{vsat}(T_1) = P_a \tag{36}$$

4.2. Intermediate compartment #2

Only vapour was considered in compartment #2. Also this compartment does not exist (*i.e.* $V_2 = 0$ and $m_2 = 0$) until water boils in compartment #1 *i.e.* $T_1 \geq 100$°C. Its pressure P_2 is assumed to be greater than P_a. To compute the mass m_2, using the state equation for ideal gas, we get:

$$m_2 = \frac{M_w \cdot P_2 \cdot V_2}{R \cdot (T_2 + T_\tau)} \tag{37}$$

In addition, convective heat transfer is balanced by enthalpy gain/loss due to vapour fluxes:

$$\begin{aligned} Cp_v \cdot \frac{d(m_2 \cdot T_2)}{dt} \quad = \quad & -\phi_{h,2\to1} \cdot A_{1,2} + \phi_{m,1\to2} \cdot A_{1,2} \cdot (L_v + Cp_v \cdot T_1) \\ & +\phi_{h,3\to2} \cdot A_{2,3} - \phi_{m,2\to a} \cdot A_{2,3} \cdot (L_v + Cp_v \cdot T_2) \end{aligned} \tag{38}$$

For the vapor mass balance, we have two conditions:

1. The heat capacity of compartment #2 is zero at the beginning, so the difference between the heat flows entering and leaving compartment #2 must exactly match the energy increase in compartment #2.

2. The difference between the mass flows entering and leaving compartment #2 is the time derivative of m_2.

We know the speed at which V_2 grows (drying of compartment #1), so pressure P_2 and temperature T_2 must satisfy both of the above conditions.

4.3. External compartment #3

4.3.1. Case 1: $I_3 > 0$, $T_3 < 0$

In this case, all the water is ice and remains at temperature below 0°C and no drying (sublimation) occurs, hence:

$$\frac{dI_3}{dt} = \frac{dW_3}{dt} = \frac{dX_3}{dt} = 0 \tag{39}$$

$$\rho_{dfm3} \cdot V_3 \cdot (Cp_{dfm3} + Cp_{ice} \cdot I_3 + Cp_w \cdot W_3) \cdot \frac{d\,(T_3)}{dt} = -\phi_{h,3\to2} \cdot A_{2,3} + \phi_{h,a\to3} \cdot A_{3,a} \tag{40}$$

where $A_{2,3}$ is the section area between compartments #2 and #3. Former equation should be written differently when compartment #2 does not exist:

$$\rho_{dfm3} \cdot V_3 \cdot (Cp_{dfm3} + Cp_{ice} \cdot I_3 + Cp_w \cdot W_3) \cdot \frac{d\,(T_3)}{dt} = -\phi_{h,3\to1} \cdot A_{2,3} + \phi_{h,a\to3} \cdot A_{3,a} \tag{41}$$

4.3.2. Case 2: $I_3 > 0$, $T_3 = 0$

In this case, the temperature is stabilised at 0°C until all the ice is transformed into liquid water:

$$\frac{dT_3}{dt} = 0 \tag{42}$$

All thermal energy taken from convection surrounding air is used either to heat compartment #1 or to melt ice into liquid water:

$$V_3 \cdot \rho_{dfm3} \cdot \frac{d\,((Cp_{dfm3} + Cp_{ice} \cdot I_3 + Cp_w \cdot W_3) \cdot T_3)}{dt} = \phi_{h,a\to3} \cdot A_{3,a} - \phi_{h,3\to1} \cdot A_{2,3} + \rho_{dfm3} \cdot V_3 \cdot \frac{dI_3}{dt} \cdot L_{defrost} \tag{43}$$

Hence, we have

$$0 = \phi_{h,a\to3} \cdot A_{3,a} - \phi_{h,3\to1} \cdot A_{2,3} + \rho_{dfm3} \cdot V_3 \cdot \frac{dI_3}{dt} \cdot L_{defrost} \tag{44}$$

which gives the following relationship::

$$\rho_{dfm3} \cdot V_3 \cdot \frac{dI_3}{dt} \cdot L_{defrost} = -\phi_{h,a\to3} \cdot A_{3,a} + \phi_{h,3\to1} \cdot A_{2,3} \tag{45}$$

At the same time, the overall mass of compartment #3 is constant (we assumed no drying until ice disappears):

$$\frac{dX_3}{dt} = 0 \;\Rightarrow\; \frac{dW_3}{dt} = -\frac{dI_3}{dt} \tag{46}$$

as well as its volume (as always for compartment #3).

4.3.3. Case 3: $I_3 = 0$, $0 < T_3 < 100$

In this case, there is no more ice ($X_3 = W_3$), $T_1 < 100$, compartment #2 does not exist yet, and the water mass transfer is a convective one:

$$\frac{d(\rho_{dfm3} \cdot V_3 \cdot X_3)}{dt} = -\phi_{m,3\to a} \cdot A_{3,a} + 0 \tag{47}$$

In addition, convective heat transfer is balanced by enthalpy gain/loss due to vapour fluxes:

$$\begin{aligned} \rho_{dfm3} \cdot V_3 \cdot \frac{d\,((Cp_{dfm3} + Cp_w \cdot W_3) \cdot T_3)}{dt} \;=\; & -\phi_{h,3\to1} \cdot A_{1,3} + \\ & \phi_{h,a\to3} \cdot A_{3,a} - \phi_{m,3\to a} \cdot A_{3,a} \cdot (L_v + Cp_v \cdot T_3) \end{aligned} \tag{48}$$

4.3.4. Case 4: $I_3 = 0$, $T_3 \geq 100$

In this case, the water ($X_3 = W_3$) can boil hence encounters no resistance to mass transfer. The water mass transfer is driven only by the heat transfer as described by the following equation:

$$\begin{aligned} \rho_{dfm3} \cdot V_3 \cdot \frac{d\left((Cp_{dfm3} + Cp_w \cdot W_3) \cdot T_3\right)}{dt} &= -\phi_{h,3\to 2} \cdot A_{2,3} + \phi_{h,a\to 3} \cdot A_{3,a} \\ &\quad -\phi_{m,3\to a} \cdot A_{3,a} \cdot (L_v + Cp_v \cdot T_3) \end{aligned} \tag{49}$$

If compartment #2 does not exist, it becomes:

$$\begin{aligned} \rho_{dfm3} \cdot V_3 \cdot \frac{d\left((Cp_{dfm3} + Cp_w \cdot W_3) \cdot T_3\right)}{dt} &= -\phi_{h,3\to 1} \cdot A_{2,3} + \phi_{h,a\to 3} \cdot A_{3,a} \\ &\quad -\phi_{m,3\to a} \cdot A_{3,a} \cdot (L_v + Cp_v \cdot T_3) \end{aligned} \tag{50}$$

In addition, one algebraic condition must be respected: the boiling curve to follow, with W_3 being a function of T_3:

$$Aw_3 \cdot P_{vsat}(T_3) = P_a \tag{51}$$

Using (18), we get

$$\begin{aligned} \rho_{dfm3} \cdot V_3 \cdot \left(Cp_{dfm3} + Cp_w \cdot W_3 + Cp_w \cdot \frac{\partial W_3}{\partial T_3} \cdot T_3\right) \cdot \frac{dT_3}{dt} &= -\phi_{h,3\to 2} \cdot A_{2,3} + \phi_{h,a\to 3} \cdot A_{3,a} \\ &\quad +\rho_{dfm3} \cdot V_3 \cdot \frac{dX_3}{dT_3} \cdot \frac{dT_3}{dt} \cdot (L_v + Cp_v \cdot T_3) \end{aligned} \tag{52}$$

We finally get

$$\begin{aligned} \rho_{dfm3} \cdot V_3 \cdot \left(Cp_{dfm3} + Cp_w \cdot W_3 + Cp_w \cdot \frac{\partial W_3}{\partial T_3} \cdot T_3 - \frac{dX_3}{dT_3} \cdot (L_v + Cp_v \cdot T_3)\right) \cdot \frac{dT_3}{dt} \\ = -\phi_{h,3\to 2} \cdot A_{2,3} + \phi_{h,a\to 3} \cdot A_{3,a} \end{aligned} \tag{53}$$

where $\frac{\partial W_3}{\partial T_3}$ is computed with equation (8), with $\frac{dAw}{dT}$ given by (51).

In case compartment #2 does not exist, it becomes:

$$\begin{aligned} \rho_{dfm3} \cdot V_3 \cdot \left(Cp_{dfm3} + Cp_w \cdot W_3 + Cp_w \cdot \frac{\partial W_3}{\partial T_3} \cdot T_3 - \frac{dX_3}{dT_3} \cdot (L_v + Cp_v \cdot T_3)\right) \cdot \frac{dT_3}{dt} \\ = -\phi_{h,3\to 1} \cdot A_{2,3} + \phi_{h,a\to 3} \cdot A_{3,a} \end{aligned} \tag{54}$$

5. Model implementation

The different events described in Table 1 were taken into account, resulting in different equation systems or one event-driven equation set. They were implemented under Matlab (version 2017b, Mathworks, USA). The systems of equations are constituted by the following ODE equations: (9), (15), (18), (23–22), (26), (30), (34), (35), (38), (40), (41), (45), (51), (49), (52), (53), (54). The `ode15s` solver was used to solve the different ODE equation systems. The options `odeset` of `ode15s` had relative tolerance `RelTol` set to 10^{-4} before compartment #1 boils, and to 10^{-7} during boiling. All physical parameters used as input for the model are listed in Table 2, including $V_1(t = 0)$, V_3 (such that

Table 2: Input parameters used in the simulations

Input parameter	Value	Unit	Reference
A	7.5		Murray (1967)
$A_{1,2}$	$4 \cdot l_1 \cdot L_1 + 2 \cdot l_1^2$	m^2	Computed
$A_{2,3}$	$17.22 \cdot 10^{-4}$	m^2	Indirect measure
$A_{3,a}$	$23.22 \cdot 10^{-4}$	m^2	Indirect measure
B	237.3	K	Murray (1967)
Cp_{ice}	2.108	$kJ \cdot kg^{-1} \cdot K^{-1}$	
Cp_w	4.186	$kJ \cdot kg^{-1} \cdot K^{-1}$	
Cp_v	1.88	$kJ \cdot kg^{-1} \cdot K^{-1}$	
Cp_{dfm1}	1.57	$kJ \cdot kg^{-1} \cdot K^{-1}$	Choi and Okos (1986)
Cp_{dfm3}	1.61	$kJ \cdot kg^{-1} \cdot K^{-1}$	Choi and Okos (1986)
$I_{m/0}$	n.d	%	Indirect measure
$I_{1/0}$	60	%	Indirect measure
$I_{3/0}$	0	%	Indirect measure
L_v	2501.0	$kJ \cdot kg^{-1}$	
$L_{defrost}$	333.0	$kJ \cdot kg^{-1}$	
L	$60 \cdot 10^{-3}$	m	Direct measure
L_1	$L - 2 \cdot l_3 - 2 \cdot l_2$	m	Computed
L_2	$L - 2 \cdot l_3 = 58 \cdot 10^{-3}$	m	Indirect measure
L_3	$60 \cdot 10^{-3}$	m	Direct measure
l	$9 \cdot 10^{-3}$	m	Direct measure
l_1	$l_0 - 2 \cdot l_3 - 2 \cdot l_2$	m	Dependent state variable
l_2	$l_2 = (l_1 - l_{1/0})/2$	m	Computed
l_3	10^{-3}	m	Direct measure
$M_{v/a}$	0.62198		Loncin and Merson (1979)
P_{vsat0^oC}	$10^{2.7858}$	Pa	Murray (1967)
$\rho_{dfm1}*$	1494	$kg \cdot m^{-3}$	Choi and Okos (1986)
$\rho_{dfm3}*$	1459	$kg \cdot m^{-3}$	Choi and Okos (1986)
ρ_w	1000	$kg \cdot m^{-3}$	
r_l	14.11		Bassal et al. (1993)
r_n	$-5.013 \cdot 10^{-2}$		Bassal et al. (1993)
r_q	0.124		Bassal et al. (1993)
r_t	$2.063 \cdot 10^{-3}$		Bassal et al. (1993)
T_τ	273.16	K	Loncin and Merson (1979)
V	$4.86\ .10^{-6}$	m^3	Indirect measure
V_1	$l_1^2 \cdot L_1$	m^3	Computed
V_2	$V_{1/0} - V_1$	m^3	Computed
V_3	$2.018.10^{-6}$	m^3	Indirect measure
$X_{m/0}$	2.330	d.b	Direct measure
$X_{1/0}$	3.000	d.b	Direct measure
$X_{2/0}$	0	d.b	Direct measure
$X_{3/0}$	1.713	d.b	Direct measure

$V = V_1 + V_2 + V_3$) and $A_{i,j}$. All calculations were performed with Matlab (version 2017b, Mathworks, USA). The typical simulation time was one second using 10^{10} bytes of memory (RAM) on a 64 bit computer with 2.30 GHz Intel(R) Core (TM) i5-62004 CPU@.

6. Testing and parameters identification

X_m, T_a, T_1, T_s and T_{IR} were measured in triplicates experiments and their median $X_{m\ exp}$, $T_{a\ exp}$, $T_{1\ exp}$, $T_{s\ exp}$ and $T_{IR\ exp}$ were computed. The standard deviation (σ_{T_1}, σ_{X_m}, ...) of measurements were computed with `std` (see error bars of $\pm$ two sigmas in Figures 4 and 5). The process was simulated taking into account the interpolation (with `interp1q`) of median $T_{a\ exp}$ of air temperatures. The function `fminsearch` were used to identify the parameters $k_{3,a}$, $h_{1,3}$, $h_{2,3}$ and $h_{3,a}$. This function minimized the root-mean-square error (RMSE) between:

- the median of experimental water content ($X_{m\ exp}$) and the prediction data (X_m), divided by the sum of 0.01 d.b. plus the experimental standard deviation.

- the median of experimental core temperature data ($T_{1\ exp}$) and the prediction data (T_1), divided by the sum of 1 Kelvin plus the experimental standard deviation.

The different parameters were identified together, minimizing the residue. The functions `nlparci` and `nlinfit` computed 95 % confidence intervals, assuming a normal noise distribution.

$$(RMSE)^2 = \sum_{All\ Experiments} \left(\sum_{All\ measurements} \left(\frac{X_{m\ exp} - X_m}{0.01 + \sigma_{X_m}} \right)^2 + \sum_{All\ measurements} \left(\frac{T_{1\ exp} - T_1}{1 + \sigma_{T_1}} \right)^2 \right) \tag{55}$$

7. State space representation

In this part, we intend to develop previous expressions in equations to obtain the canonical ODE system $\frac{d\vec{x}}{dt} = f(\vec{x}, \vec{u})$ with here $\vec{x}$ being the vector of state variables (*i.e.* I_1, W_1, T_1, V_1, T_2, V_2, I_3, W_3, T_3) and $\vec{u}$ being the vector of external conditions (*i.e.* RH_a and T_a). The final state in the program contains $I_1, W_1, T_1, I_3, W_3, T_3, T_2, P_2, V_1$.

Before compartment #1 boils, the actual state variable is [I_1, W_1, T_1, I_3, W_3, T_3]. After compartment #1 has started boiling, $\vec{x}$ is a vector mixing state variables (*i.e.* P_2, T_1, T_2, W_3, T_3) with time dependent width l_1 and volume V_1. Due to -solver related- numerical problems caused by the shrinkage of compartment #1, The value for l_1 is enhanced at each timestep with one loop of Newton optimization from the value of V_1 with

$$l_{1better} = l_1 + \frac{V_1 - l_1^2 \cdot L_1}{\frac{dV_1}{dl_1} \cdot (l_1)} \tag{56}$$

where $L_1 = L_{1/0} - l_{1/0} + l_1$ and

$$\frac{dV_1}{dl_1}(l_1) = 2 \cdot l_1 \cdot L_1 + l_1^2. \tag{57}$$

This Newton loop doubles the number of significant digits. The enhancement is also fed back to the current estimation of l_1 with

$$\frac{dl_1}{dt} = \frac{\frac{dV_1}{dt}}{\frac{dV_1}{dl_1}(l_{1better})} + \frac{l_{1better} - l_1}{\tau_1} \tag{58}$$

with a characteristic time of $\tau_1 = 0.1$ seconds, which is a trade-off because if τ_1 is too slow, the ODE solver stalls, and if it is too high, the state variable is left behind too far away to get more than two significant digits of precision. Another possible workaround with high characteristic time τ_1 would be to perform multiple optimization of newton loops, but this workaround sometimes does not converge. The extreme case of setting the characteristic time to infinity is identical to the case without l_1 in the state variable, and it did suffer from the problem of convergence. At last resort, we could have used Cardano's formula, but that would have too much suffered from instabilities due to the relative precision of other state variables. Another way out would have been to use DAE solvers, which would have simplified the model but with poorer precision. Approximating the volume with a second degree polynomial and using a Newton loop was also tested, and resulted in random imprecisions. The trade-off of adding l_1 aside of the state variable was proved reliable. The initial value for l_1 is deduced from V_1 by solving $l_{1better} = l_1$.

8. Results and discussion

To estimate the parameters of the model, the simulation output was compared to experimental data. Three different hot-air frying conditions were simulated (Table 3). Since temperature profiles and water loss can be measured, these were used for the comparison. In addition, the temperature and water content of the french fries were also used as relevant quality parameters of the final product.

Table 3: Air velocity and energy consumed by the fryer in different conditions

Setting	Air velocity, $m{\cdot}s^{-1}$	Halogen	Mass energy consumption (MEC), $kJ{\cdot}kg^{-1}$ of water vapor
C-Standard	4 (Standard)	No	7312
C-Standard-Halo	4 (Standard)	Yes	7508
High Convection	6 (High)	No	7878

$$\text{MEC} = \frac{\text{kJ consumed to heating air}}{\text{kg of evapored water}} \tag{59}$$

The energy consumed by the frying equipment was measured during the frying process under the three experimental conditions. Knowing the evolution of water loss, the mass energy consuption (MEC, equation 59) was calculated as the quantity of energy (kJ/kg) needed by the frying equipment to evaporate 1 kg of water. The three frying conditions differ in the energy consumption trajectories.

Figure 3 shows that energy consumption increases with heating time for all the three frying conditions. The analysis of the energy consumption trajectories shows that the three frying conditions are different in terms of how they provide energy to the product. For each, the initial energy consumption rate was very high (C-Standard: 1.67 kW; C-Standard-Halo: 2.39 kW; and High Convection: 1.83 kW)

to allow respectively a heating rate of 22.7 °C/min, 62.7 °C/min and 20.3 °C/min to reach the set temperature of the fryer but also for heating the potato fry. The air temperature reached 180 °C in 50 — 108 seconds depending on the frying conditions. C-Standard-Halo condition recorded the shortest heating period (50 s). After this period, controllers set on or off the heating systems to compensate the loss of energy due to air exchange and the cooking of the product. Therefore the mean energy consumption rate decreased to 1.08 kW, 1.12 kW, and 1.43 kW to maintain the air temperature at 180 °C, for C-Standard, C-Standard-Halo, and High Convection, respectively.

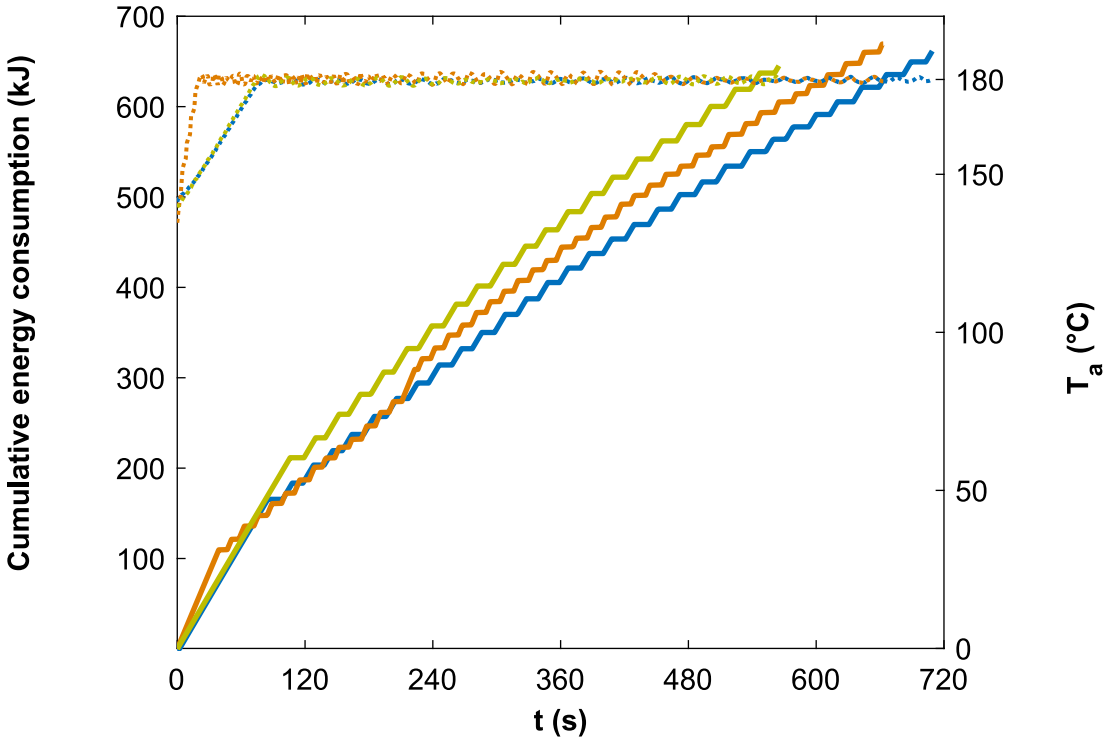

Figure 3: Experimental data of air temperature (dashed line) and cumulative energy consumption (solid line) of the fryer with continuous heating time for different frying conditions.
— C-Standard
— C-Standard-Halo
— High Convection

8.1. Heat and mass transfer coefficient

To further assess the validity of the model, the heat transfer coefficients were evaluated. The identified heat and mass transfer coefficients are shown in Table 4. The $k_{3,a}$ identified correspond to the mass transfer coefficients of the convective drying phase in compartment #3. Generally, the mass transfer coefficient is a function of the moisture gradient and the frying temperature. As water saturation decreases, the mass transfer coefficient decreases, and as the frying temperature increases, the initial mass transfer coefficient increases. Available literature do not provide many values for the mass transfer coefficient for potato products. The identified values for $k_{3,a}$ are reasonable ($3.58 \cdot 10^{-3}$ to $4.10 \cdot 10^{-3}$ m·s^{-1}), but remain high compared to the values found in the case of conventional drying. Due to different conditions of the drying process, it would be difficult to compare the value of the mass transfer coefficient identified in this study with reference data. Most authors (Miketinac et al.,

1992; Białobrzewski, 2007; Dhalsamant et al., 2017) use a difference in water content in mass as the driving force for the water flux density, and the values of the mass transfer coefficient obtained are generally in the magnitude of 10^{-5} — 10^{-4} m·s^{-1}. While in our formulation (equation 9) based on volume concentration, the values of the mass transfer coefficient are in the magnitude of 10^{-3} m·s^{-1}. The processing conditions during hot-air frying are also more drastic, with high air flow velocity and air temperature (180°C). Dhalsamant et al. (2017) reported that during natural convection solar drying of potato at a temperature of 34.90°C, the mass transfer coefficient was $5.16 \cdot 10^{-7}$ — $2.64 \cdot 10^{-7}$ m·s^{-1}. Miketinac et al. (1992) reported that during drying a layer of barley at an air temperature of 75 °C and at an air flow velocity of 0.56 m·s^{-1}, the value of the mass transfer coefficient was $1.08 \cdot 10^{-6}$ m·s^{-1}. Białobrzewski (2007) reported that during hot-air-drying of celery root under natural convection conditions (air temperature = 49 °C), the mass transfer coefficient was $1.40 \cdot 10^{-4}$ m·s^{-1}.

Table 4: Identified parameters for the heat transfer ($h_{1,3}$, $h_{2,3}$, $h_{3,a}$) and the water transfer ($k_{3,a}$)

Parameter	Setting	Identified value	Unit
$h_{1,3}$	All	254 ± 9	W·m^{-2}·K^{-1}
$h_{2,3}$	All	202 ± 5	W·m^{-2}·K^{-1}
$h_{3,a}$	C-Standard	66 ± 1	W·m^{-2}·K^{-1}
$h_{3,a}$	C-Standard-Halo	73 ± 1	W·m^{-2}·K^{-1}
$h_{3,a}$	High Convection	76 ± 1	W·m^{-2}·K^{-1}
$k_{3,a}$	C-Standard	$3.70 \cdot 10^{-3} \pm 0.06 \cdot 10^{-3}$	m·s^{-1}
$k_{3,a}$	C-Standard-Halo	$4.10 \cdot 10^{-3} \pm 0.06 \cdot 10^{-3}$	m·s^{-1}
$k_{3,a}$	High Convection	$3.58 \cdot 10^{-3} \pm 0.20 \cdot 10^{-3}$	m·s^{-1}

Analysis of the table 4 shows that despite the different modes of heat transfer, the gobal heat transfer coefficients remains still quite similar. The frying mode with High Convection provides a higher global heat transfer coefficient (High Convection, $h_{3,a} = 96$ W·m^{-2}·K^{-1}). The surface temperature and vapour flux also change faster than the other modes. The higher is $h_{3,a}$, the faster the product temperature reaches 100 °C and the higher it rises at the end of the frying process (figure 4). The model is therefore very sensitive to the convective heat transfer coefficient between the external compartment and the hot-air. The heat transfer coefficients obtained are extremely far from the values that can be obtained in the deep-fat frying process, which can be up to 250 — 1000 (W·m^{-2}·K^{-1}). But this model can simulate different frying operating conditions in order to optimize the hot-air frying operation.

The internal transfer coefficients ($h_{1,3}$ and $h_{2,3}$) are four times the external transfer coefficients ($h_{3,a}$). Thus, internal heat transfer is not limiting.

Five powers of 0.1 (10^{-10} to 10^{-14}) were tested for intrinsic permeability κ_v of the compartment #3 medium to vapour (m_2). This had negligible effects on the model predictions.

8.2. Temperature profiles

The figure 4 displays the experimental and simulated evolution of french fry temperature during frying for the differents geometrical points. The mean coefficient of variation for experimental temperature acquisition inside french fry was quite good (< 10 °C). The root-mean-square error between experimental and predicted values was reasonable as well. The figure 4 shows also the evolution of the air temperature in the oven away from the french fries, as well as that of the core and surface of the french fries as a function of time. The air temperature close to the french fries rises rapidly to 150 °C,

then gradually reaches 180 °C in less than 120 seconds of cooking. The evolution of the -estimated-actual surface temperature is represented by an area between the $T_{IR\ exp}$ measured by infrared and the $T_{s\ exp}$ measured by a thermocouple. The surface temperature of the french fries increases relatively rapidly over time due to the high initial temperature difference between the hot-air and the frozen french fries. To reach 100 °C on the surface of the french fry, at least 100 to 120 seconds of frying are required instead of 20 seconds for deep-fat frying (Achir et al., 2008; van Koerten et al., 2017). This is related to the higher

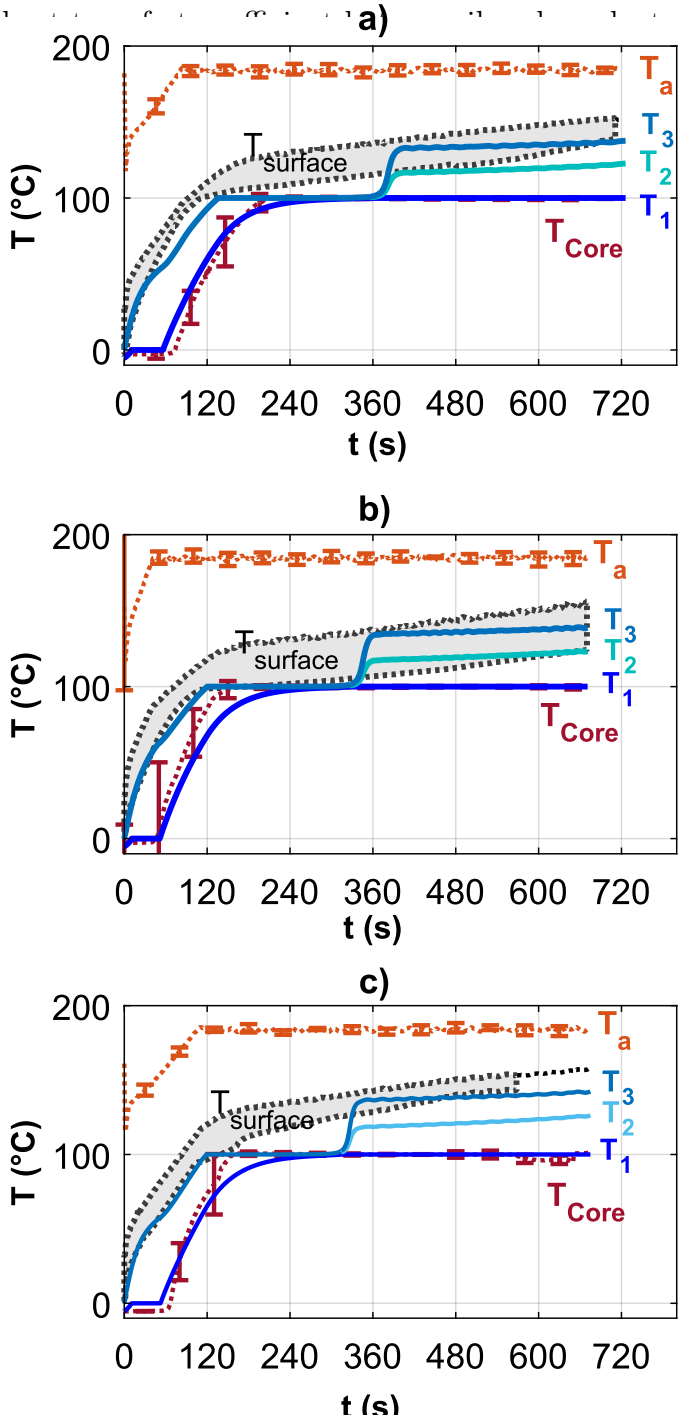

Figure 4: The measured evolution of temperatures in time plotted for the core (T_{co}) and the surface of the french fries (T_s) in three different air-frying conditions: a) C-Standard, b) C-Standard-Halo, and c) High Convection. The solid lines represent the model predictions and the dashed lines represent the experimental data. T_a = Air temperature in the area around the french fries and T_1, T_2, and T_3 correspond to the temperatures of compartment #1, #2 and #3 respectively. Error bars represent twice (2×) standard deviation between replicates.

The experimental core temperature shows a plateau around –4 °C at the beginning of frying. This plateau is linked to the core defrosting which occurs in less than 60 s. This plateau do not fit well with the simulation data because we assumed that defrosting occured at 0 °C while in practice, food

defrosting takes place at temperatures below 0 °C. This hypothesis could lead to a slight mismatch in the evolution of the simulated core temperature with the experimental core temperature. Due to the resistance to heat transfer in the crust compartment (compartment #3), the temperature increase in the core compartment (compartment #1) is delayed compared to the compartment #3. However, it finally reaches a value around 100 °C, which is maintained due to the high latent heat of evaporation of water which is present in large amounts in the core. This boiling temperature, in the core, is reached after about 120 s of frying.

The same plateau is observed for the surface temperature, but the duration is much shorter than for the core: the temperature increase is halfed for a few seconds. The reason for this is the rapid dehydration of the compartment #3 close to the hot-air. When all the water has evaporated, this compartment can no longer serve as an energy sink and the temperature begins to rise. The temperature increase in the compartment #3 is well below the temperature of the hot-air near to the french fries. This is because the water located deeper inside the fry still acts as a cooling source. This plateau can also be observed in the case of deep-fat frying (5 s) but the duration of the plateau is very short compared to hot-air frying (Farid and Kizilel, 2009; Lioumbas and Karapantsios, 2012; Lalam et al., 2013; van Koerten et al., 2017).

The model predictions of the temperature for the different frying conditions are also shown in the figure 4, along the measurements. The model provides reasonable description of the temperature evolution in both the core (compartment #1) and the surface (compartment #3) for all data sets. It can be observed that the model values of the temperatures in the compartment #3 (Surface) have a plateau at 100°C for a few minutes: non-invasive techniques (Touffet et al., 2020) showed that mechanical fractures and cracks (with cavitation) occur beneath the rigid (glassy) crust, causing this discrepancy. The aim of our work is to be able to simulate both heat and mass transfer for control and optimization purposes, hence we want to stay more at the macroscopic level and consider each compartment of french fries homogenous. This is a direct consequence of the explicit incorporation of the water evaporation rate in the model. As the water in a numerical slice evaporates, the temperature will remain virtually constant. In this study, the crust thickness considered (compartment #3) is 1 mm. T_3 is therefore an average of the temperature in compartment #3, which started to increase when all the water was evaporated in the compartment #3. T_3 increases faster in the case of High Convection and C-Standard-Halo frying compared to frying under C-Standard conditions (figure 4).

Analysis of the pressure evolution at the core of the french fry, shows that P_2 is very close to P_a (overpressure < 0.5 kPa). This result supports the assumption that $P_1 = P_a$. This overpressure in hot-air frying is very low compared to the overpressure observed during deep-fat frying ($\Delta P_a > 30$ kPa)(Patsioura et al., 2016; Vauvre et al., 2014).

8.3. Water content

Figure 5 shows the mean water content kinetics of french fry for three different frying conditions experimentally measured (dashed line) and predicted by the model (solid line). The model fitted the experimental data very well. The assumption of drying of the compartment #3 before boiling is relevant, allowing to fit the first drying phase.

During the drying of food materials, water is removed from the system, causing significant shrinkage (Kawas and Moreira, 2001; Yamsaengsung and Moreira, 2002). However, in the case of frozen french fries, the global shrinkage of french fries is very small (Gouyo et al., 2021). It was not observed

a global shrinkage higher than 10 % in both radial and longitudinal direction. Therefore the mechanical effect of heat and mass transfer was neglected. The shrinkage is more related to the volume of compartment #1 (V_1). This shrinkage is reflected in equation 1, which considers that a volume of water lost in compartment #1 produces a shrinkage of the same volume (Gouyo et al., 2021).

Figure 5 shows that at the beginning of frying, there is a stage that corresponds to the rise the heating and the defrosting phase of the french fries (phase 1, the initial heating period). During this stage, the temperature of the compartment #3 is raised to the boiling temperature of the water, after which evaporation begins. Obviously, this stage lasts longer if the heat transfer coefficient (h_{3a}) is lower. This was observed only for the C-Standard condition. This first phase of drying is followed by dehydration of the product to reach a maximum around 300 to 400 s. The first dehydration slope observed on the drying curve (figure 5) corresponds to the evaporation phase in compartment #3 and the rise in temperature in compartment #1. After the water of compartment #3 has been evaporated, the temperature T_3 will exceed the boiling point of water (figure 4). The second slope corresponds to the maximum water evaporation, which coincides with the boiling phase in the compartment #1. The rate of evaporation is at its highest at this moment because both compartments #1 and #3 are boiling and additionally there is more water in compartment #1. The maximum value of the measured vapour flow density for the different hot-air frying conditions was relatively lower ($2.5 \cdot 10^{-3}$ kg·m^{-2}·s^{-1}) than what was found in deep-fat frying (5 — 10·10^{-3}kg·m^{-2}·s^{-1}) (Costa and Oliveira, 1999; Vitrac et al., 2002; Ziaiifar, 2008; van Koerten et al., 2017). In spite of the different evolution of the surface temperature for the three frying conditions, the evolution of the water loss remains very close.

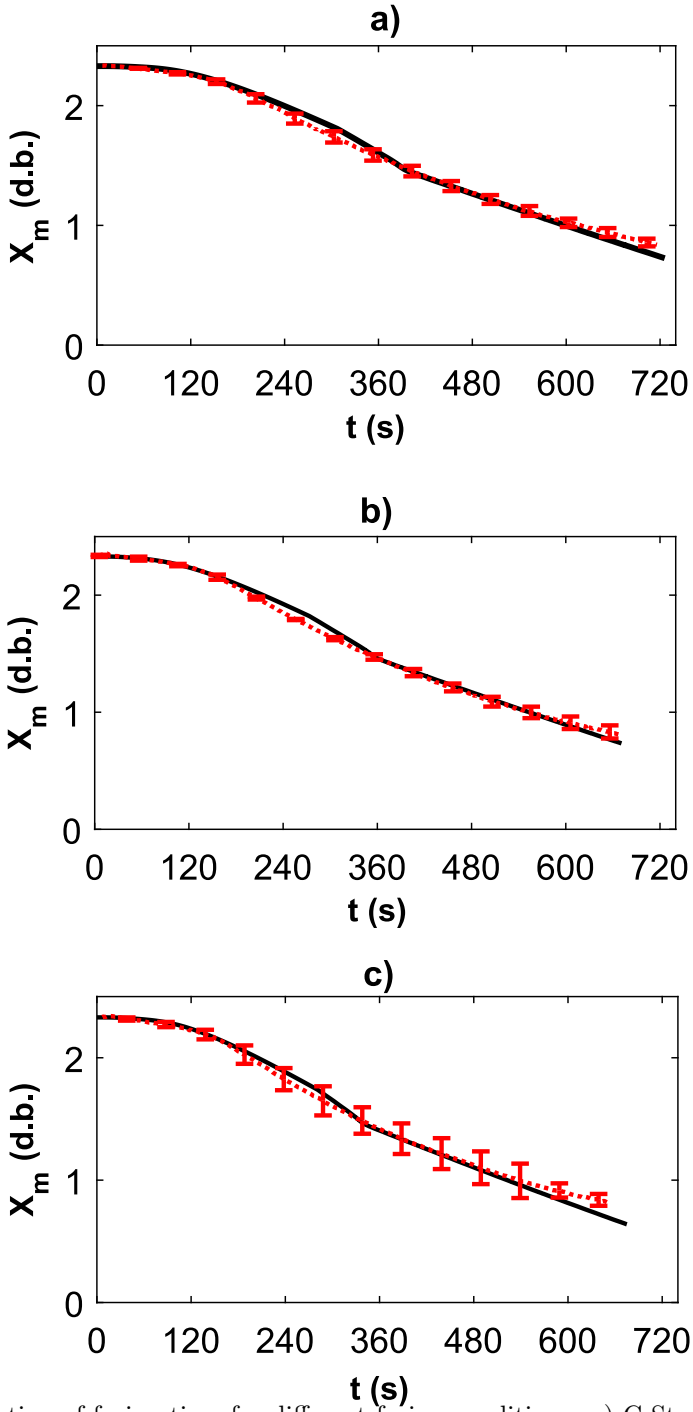

Figure 5: Water loss as function of frying time for different frying conditions: a) C-Standard, b) C-Standard-Halo, and c) High Convection. Experimental data are represented by dashed line (.....) and model predictions by a solid line (—). Error bars represent twice (2×) standard deviation between replicates.

9. Conclusion

A dynamic three-compartment model including heat and vapour transfer was developed. The model takes into account four major stages: defrosting, warm-up, convective drying and boiling drying. The proposed compartmental model showed very good fit with the experimental data of water content and core temperature evolution during hot-air frying. The model is hence accurate to describe hot-air frying of frozen -pre-fried- french fries at different conditions and can well represent the behaviour of the frozen pre-fried french fries from defrosting, warming-up to convective drying and boiling drying of the crust and boiling drying of the core. It also allows to better take into account the effect of variable air characteristics and study different ways of providing energy to the product. The model is very sensitive to the convective heat transfer coefficient between the external compartment and the hot-air, hence it can be a promising tool for the control and optimization of hot-air frying.

10. Nomenclature

A	Oswin parameter
$A_{i,j}$	contact surface of compartment i and j (m^{-2})
Aw	water activity
B	Oswin parameter
Cp	specific heat ($J{\cdot}kg^{-1}{\cdot}K^{-1}$)
h	heat transfer coefficient ($W{\cdot}m^{-2}{\cdot}K^{-1}$)
I	ice content (kg water^{-1}·kg dry fatted basis)
k_v	shrinkage parameter (m^3·kg water^{-1} ·kg dry fatted matter)
$k_{3,a}$	mass transfer coefficient ($m{\cdot}s^{-1}$)
L_i	length of compartment #i (m)
L_v	latent heat of evaporation ($J{\cdot}kg^{-1}$)
$L_{defrost}$	latent heat of fusion ($J{\cdot}kg^{-1}$)
l_0	width of potato french fry (m)
l_i	thickness of compartment #i (m)
M	molecular weight ($kg{\cdot}mol^{-1}$)
m	mass of french fries (kg)
P_a	atmospheric pressure (Pa)
P_v	partial pressure of vapour (Pa)
P_{vsat}	saturation pressure of water (Pa)
q	intermediate to compute Aw from X
r	coefficients of sorption Oswin model
R	universal gas constant ($J{\cdot}kg^{-1}{\cdot}K^{-1}$)
RH	relative humidity (%)
RMSE	Root means square error
T	temperature (°C)
t	time (s)
V	volume (m^{-3})
W	liquid water content (dry basis)
X	water content (dry basis)
Y	air water content ($kg{\cdot}kg^{-1}$)

10.1. Greek symbols

μ	dynamic viscosity (Pa·s)
κ_v	intrinsic permeability ($m{\cdot}s^{-1}$)
$\rho*$	intrinsic density ($kg{\cdot}m^{-3}$)
ϕ_h	heat flux density ($kW{\cdot}m^{-2}{\cdot}$)
ϕ_m	water flux density ($kg{\cdot}m^{-2}{\cdot}s^{-1}$)
σ	standard deviation of measurements on triplicate experiments
τ	characteristic time of enhancement of the computed width (s)
ΔP	pressure difference (Pa)

10.2. Subscripts

0	initial
0°C	at 0°C
/0	initial
/a	ratio with dry air
1	compartment #1
2	compartment #2
3	compartment #3
,	interface of compartment
$\rightarrow$	direction of transfer
a	air
$better$	better estimation
co	core
cr	crust
dfm	dry fat matter
db	db dry basis
$defrost$	defrost
eq	equilibrium
exp	median of measurements on triplicate experiments
h	relative to heat phenomena
ice	ice
i	compartment #i
IR	surface, measured by infrared
j	compartment #i
l	$100 \cdot X$ at $Aw = \frac{1}{2}$ and T=0 °C
m	relative to mass phenomena
n	dependence of $100 \cdot X$ on T at $Aw = \frac{1}{2}$
p	a power of $\frac{Aw}{1-Aw}$ in X
r	$100 \cdot X$ at $Aw = \frac{1}{2}$
s	surface
t	dependence on T of power of $\frac{Aw}{1-Aw}$ in X
τ	triple point of water
v	water vapor
$vsat$	saturated water vapor
w	water

11. Acknowledgements

The authors would like to thank the anonymous reviewers for their valuable comments.

12. Bibliographic references

References

Achir, N., Vitrac, O., Trystram, G., 2008. Simulation and ability to control the surface thermal history and reactions during deep fat frying. Chemical Engineering and Processing: Process Intensification 47, 1953–1967. doi:10.1016/j.cep.2008.03.004.

Aguilera, J.M., Gloria-Hernandez, H., 2000. Oil Absorption During Frying of Frozen Parfried Potatoes. Journal of Food Science 65, 476–479. doi:10.1111/j.1365-2621.2000.tb16031.x.

Andrés, A., Arguelles, A., Castelló, M.L., Heredia, A., 2013. Mass Transfer and Volume Changes in French Fries During Air Frying. Food and Bioprocess Technology 6, 1917–1924. doi:10.1007/s11947-012-0861-2.

Bassal, A., Vasseur, J., Loncin, M., 1993. Sorption Isotherms of Food Materials Above 100°C. LWT - Food Science and Technology 26, 505–511. doi:10.1006/fstl.1993.1100.

Białobrzewski, I., 2007. Determination of the mass transfer coefficient during hot-air-drying of celery root. Journal of Food Engineering 78, 1388–1396. doi:10.1016/j.jfoodeng.2006.01.011.

Bouchon, P., Aguilera, J.M., 2001. Microstructural analysis of frying potatoes. International Journal of Food Science and Technology 36, 669–676. doi:10.1046/j.1365-2621.2001.00499.x.

Bouchon, P., Pyle, D., 2005. Modelling oil absorption during post-frying cooling. Food and Bioproducts Processing 83, 253–260. doi:10.1205/fbp.05115.

Choi, Y., Okos, M., 1986. Food Engineering and Process Applications. volume 1. Elsevier.

Costa, R.M., Oliveira, F.A.R., 1999. Modelling the kinetics of water loss during potato frying with a compartmental dynamic model. Journal of Food Engineering 41, 177–185. doi:10.1016/S0260-8774(99)00095-3.

Costa, R.M., Oliveira, F.A.R., Delaney, O., Gekas, V., 1999. Analysis of the heat transfer coefficient during potato frying. Journal of Food Engineering 39, 293–299. doi:10.1016/S0260-8774(98)00169-1.

Courtois, F., Trystram, G., Lemaire, R., Wack, A.L., 1998. Modelling of deep fat frying of banana using a compartmental approach and boiling's theory, in: Drying '98.

Debnath, S., Rastogi, N.K., Krishna, A.G.G., Lokesh, B.R., 2009. Oil partitioning between surface and structure of deep-fat fried potato slices: A kinetic study. LWT - Food Science and Technology 42, 1054–1058. doi:10.1016/j.lwt.2009.01.006.

Dhalsamant, K., Tripathy, P.P., Shrivastava, S.L., 2017. Moisture transfer modeling during solar drying of potato cylinders considering shrinkage. International Journal of Green Energy 14, 184–195. doi:10.1080/15435075.2016.1256290.

Dincer, I., Yildiz, M., 1996. Modelling of thermal and moisture diffusions in cylindrically shaped sausages during frying. Journal of Food Engineering 28, 35–44. doi:10.1016/0260-8774(95)00026-7.

Dueik, V., Robert, P., Bouchon, P., 2010. Vacuum frying reduces oil uptake and improves the quality parameters of carrot crisps. Food Chemistry 119, 1143–1149. doi:10.1016/j.foodchem.2009.08.027.

Farid, M., Kizilel, R., 2009. A new approach to the analysis of heat and mass transfer in drying and frying of food products. Chemical Engineering and Processing: Process Intensification 48, 217–223. doi:10.1016/j.cep.2008.03.013.

Farid, M.M., Chen, X.D., 1998. The analysis of heat and mass transfer during frying of food using a moving boundary solution procedure. Heat and Mass Transfer 34, 69–77. doi:10.1007/s002310050233.

Farkas, B.E., Singh, R.P., Rumsey, T.R., 1996. Modeling heat and mass transfer in immersion frying. II, model solution and verification. Journal of Food Engineering 29, 227–248. doi:10.1016/0260-8774(95)00048-8.

Garayo, J., Moreira, R., 2002. Vacuum frying of potato chips. Journal of Food Engineering 55, 181–191. doi:10.1016/S0260-8774(02)00062-6.

Gouyo, T., Rondet, E., Mestres, C., Hofleitner, C., Bohuon, P., 2021. Microstructure analysis of crust during deep-fat or hot-air frying to understand French fry texture. Journal of Food Engineering 298, 110484. doi:10.1016/j.jfoodeng.2021.110484.

Grenier, D., Bohuon, P., Méot, J.M., Baillères, H., 2010. Insights into fry-drying process of wood through a simplified approach of heat and mass transport phenomena. Chemical Engineering and Processing: Process Intensification 49, 490–499. doi:10.1016/j.cep.2010.03.016.

Heredia, A., Castelló, M.L., Argüelles, A., Andrés, A., 2014. Evolution of mechanical and optical properties of French fries obtained by hot air-frying. LWT - Food Science and Technology 57, 755–760. doi:10.1016/j.lwt.2014.02.038.

Hubbard, L.J., Farkas, B.E., 1999. A method for determining the convective heat transfer coefficient during immersion frying. Journal of Food Process Engineering 22, 201–214. doi:10.1111/j.1745-4530.1999.tb00481.x.

Kawas, M.L., Moreira, R.G., 2001. Effect of Degree of Starch Gelatinization on Quality Attributes of Fried Tortilla Chips. Journal of Food Science 66, 300–306. doi:10.1111/j.1365-2621.2001.tb11336.x.

van Koerten, K., Schutyser, M., Somsen, D., Boom, R., 2015. A pore inactivation model for describing oil uptake of french fries during pre-frying. Journal of Food Engineering 146, 92–98. doi:10.1016/j.jfoodeng.2014.09.010.

van Koerten, K.N., Somsen, D., Boom, R.M., Schutyser, M.A.I., 2017. Modelling water evaporation during frying with an evaporation dependent heat transfer coefficient. Journal of Food Engineering 197, 60–67. doi:10.1016/j.jfoodeng.2016.11.007.

Lalam, S., Sandhu, J.S., Takhar, P.S., Thompson, L.D., Alvarado, C., 2013. Experimental study on transport mechanisms during deep fat frying of chicken nuggets. LWT - Food Science and Technology 50, 110–119. doi:10.1016/j.lwt.2012.06.014.

Lioumbas, J.S., Karapantsios, T.D., 2012. Effect of Potato Orientation on Evaporation Front Propagation and Crust Thickness Evolution during Deep-Fat Frying. Journal of Food Science 77, E297–E305. doi:10.1111/j.1750-3841.2012.02915.x.

Loncin, M., Merson, R.L., 1979. Food engineering, principles and selected applications. Academic Press, New York.

Miketinac, M., Sokhansanj, S., Tutek, Z., 1992. Determination of heat and mass transfer coefficients in thin layer drying of grain. Transactions of the American Society of Agricultural Engineers 35, 1853–1858. doi:10.13031/2013.28806. cited By 47.

Murray, F.W., 1967. On the computation of saturation vapor pressure. Journal of Applied Meteorology 6, 203–204. doi:10.1175/1520-0450(1967)006<0203:OTCOSV>2.0.CO;2.

Ni, H., Datta, A., 1999. Moisture, oil and energy transport during deep-fat frying of food materials. Food and Bioproducts Processing 77, 194–204. doi:10.1205/096030899532475.

Oswin, C.R., 1946. The kinetics of package life. iii. the isotherm. Journal of the Society of Chemical Industry 65, 419–421. doi:https://doi.org/10.1002/jctb.5000651216.

Patsioura, A., Vauvre, J.M., Kesteloot, R., Smith, P., Trystram, G., Vitrac, O., 2016. Chapter 17 - Mechanisms of Oil Uptake in French Fries, in: Singh, J., Kaur, L. (Eds.), Advances in Potato Chemistry and Technology (Second Edition). Academic Press, San Diego, pp. 503–526. doi:10.1016/B978-0-12-800002-1.00017-0.

Pedreschi, F., 2009. Fried and Dehydrated Potato Products, in: Advances in Potato Chemistry and Technology. Elsevier, pp. 319–337. doi:10.1016/B978-0-12-374349-7.00011-8.

Pedreschi, F., Aguilera, J.M., 2002. Some changes in potato chips during frying observed by confocal laser scanning microscopy (CLSM). Food Science and Technology International 8, 197–201. doi:10.1177/1082013202008004931.

Sansano, M., Juan-Borrás, M., Escriche, I., Andrés, A., Heredia, A., 2015. Effect of Pretreatments and Air-Frying, a Novel Technology, on Acrylamide Generation in Fried Potatoes. Journal of Food Science 80, T1120–T1128. doi:10.1111/1750-3841.12843.

Sumnu, S.G., Sahin, S., 2008. Advances in Deep-Fat Frying of Foods. CRC Press.

Teruel, M.R., Gordon, M., Linares, M.B., Garrido, M.D., Ahromrit, A., Niranjan, K., 2015. A comparative study of the characteristics of french fries produced by deep fat frying and air frying. Journal of Food Science 80, E349–E358. doi:10.1111/1750-3841.12753.

Tian, J., Chen, S., Shi, J., Chen, J., Liu, D., Cai, Y., Ogawa, Y., Ye, X., 2017. Microstructure and digestibility of potato strips produced by conventional frying and air-frying: An in vitro study. Food Structure 14, 30–35. doi:10.1016/j.foostr.2017.06.001.

Touffet, M., Trystram, G., Vitrac, O., 2020. Revisiting the mechanisms of oil uptake during deep-frying. Food and Bioproducts Processing 123, 14 – 30. doi:https://doi.org/10.1016/j.fbp.2020.06.007.

Vauvre, J.M., Kesteloot, R., Patsioura, A., Vitrac, O., 2014. Microscopic oil uptake mechanisms in fried products. European Journal of Lipid Science and Technology 116, 741–755. doi:10.1002/ejlt.201300278.

Vitrac, O., Dufour, D., Trystram, G., Raoult-Wack, A.L., 2002. Characterization of heat and mass transfer during deep-fat frying and its effect on cassava chip quality. Journal of Food Engineering 53, 161–176. doi:10.1016/S0260-8774(01)00153-4.

Xiong, X., Narsimhan, G., Okos, M.R., 1992. Effect of composition and pore structure on binding energy and effective diffusivity of moisture in porous food. Journal of Food Engineering 15, 187–208. doi:10.1016/0260-8774(92)90050-G.

Yamsaengsung, R., Moreira, R.G., 2002. Modeling the transport phenomena and structural changes during deep fat frying: Part I: model development. Journal of Food Engineering 53, 1–10. doi:10.1016/S0260-8774(01)00134-0.

Ziaiifar, A.M., 2008. Mécanisme d'imprégnation en huile au cours de friture. thesis. Paris, AgroParisTech.